Model updating of an oblique multi-span railway bridge and effect of transverse diaphragms on the dynamic performance

J.C. Sánchez-Quesada [1], **E. Moliner** [1], **A. Romero** [2], **P. Galvín** [2], **M.D. Martínez-Rodrigo** [1]
[1] Universitat Jaume I, Departamento de ingeniería mecánica y construcción,
Avda. Sos baynat s\n, ES-12071, Castellón de la Plana, Spain

[2] Universidad de Sevilla, Escuela técnica superior de Ingeniería,
Camino de los Descubrimientos s\n, ES-41092, Sevilla, Spain
e-mail: **jquesada@uji.es**

Abstract
This paper adresses the dynamic response of skewed multi-span railway bridges composed by simply-supported pre-stressed concrete girder decks. This deck typology is usually characterised by the presence of transverse diaphragms at the span ends to increase the torsional stiffness. In skewed decks, the dynamic response is significantly affected by the boundary conditions, and occasionally the transverse diaphragms are not executed in the existing structures. Preliminary studies performed by the authors concluded that these elements could affect the dynamic performance. In this contribution this former study is completed using a detailed 3D model of an existing structure, which is updated with experimental measurements. Adittionally, several model variants have been developed to evaluate the combined effect of different levels of obliquity and transverse diaphragms configurations on the dynamic response. Finally, a numerical-experimental comparison of the bridge response under operating conditions is presented.

1 Introduction

The dynamic behaviour of railway bridges has been a matter of concern for scientists and engineers during the past decades. The periodic nature of the railway excitation, associated to the succession of identical passenger coaches travelling at constant speed, may cause important vibrations at the deck level induced by resonance phenomena. Harmful consequences such as ballast destabilization, increase of maintenance costs of the track, passenger discomfort and, in the worst-case scenario, risk of derailment, may be derived from an excessive level of vertical vibrations. For these reasons, current standards such as Eurocode (EC) [1] limit the maximum vertical accelerations at the deck level to 3.5m/s^2 for ballasted tracks. This constitutes a considerably restrictive requirement for the design or assessment of short-to-medium span simply-supported (SS) bridges, which are prone to experience important acceleration levels due to their usually associated low mass [2, 3].

In railway bridges composed of SS spans the dynamic response is generally dominated by the contribution of the first longitudinal bending mode [4, 5]. However, in the case of multi-track bridges with oblique decks and similar span length to deck width ratio, the contribution of other modes such as torsion or transverse bending may be notable. In these cases, the use of three-dimensional structural models becomes necessary and their adjustment is very sensitive to boundary conditions. This work is focuses on the dynamic response of girder bridges, typically found in short-to medium span lengths of both conventional and high-speed railway lines, with significant skewness. Attention will be given to the influence of diaphragms at the end sections and to the participation of modal contributions different from the longitudinal bending ones on the acceleration response.

In this context, previous works have evaluated the dynamic performance of skewed railway bridges [6], showing the sensitivity of the model to the boundary conditions. Also Nguyen et al. [7] evaluated the dynamic response of skewed bridges subjected to moving loads with a simplified numerical model based on beam theory, concluding that the skewness plays an important role on the dynamic deflections. Moliner et al. [8] analysed the influence of end diaphragms in skewed bridges on the modal parameters and on the train induced vibrations using simplified plate-beam models. The authors concluded that the presence of these elements leads to an increase in the natural frequencies, especially of the modes with significant deformation of the cross section. They also pointed out a reduction of the deck maximum acceleration levels under high speed (HS) traffic with the end diaphragms, especially in the case of oblique decks with a small number of longitudinal girders.

Most of the works devoted to this topic neglect in the numerical models the presence of the track. Physically, the ballasted track distributes the axle loads from the rails to the structure, acts as high-frequency filter, may induce a restraining effect at the end sections of each span due to the rail continuity and also experimental evidences of coupling mechanisms exerted by the ballast layer between either consecutive spans or adjacent SS decks have been reported [9, 10, 11]. Therefore, the inclusion of the ballasted track in the numerical models permits a more realistic representation of the dynamic response of the structure, which can be particularly relevant for those bridge typologies that exhibit a dynamic behaviour significantly affected by the boundary conditions, as it is the case of skewed decks.

Based on the previous considerations, the present work aims to investigate the dynamic performance of oblique railway bridges composed by SS spans and girder decks with end diaphragms. To this end, a three-dimensional (3D) detailed finite element (FE) model of an existing and representative skewed bridge belonging to the Spanish HS railway network, Jabalón HS railway bridge, is implemented and updated with experimental measurements. Based on this reference case, a number of model variants are implemented covering (i) several levels of obliqueness and (ii) three transverse diaphragm configurations. Next, the maximum dynamic response under operating conditions for each case of study is evaluated under the passage of the High Speed Load Model-A (HSLM-A) trains from Eurocode 1 (EC1) [5]. Special attention is given to the participation of modes different from the longitudinal bending ones. Finally, the response of Jabalón HS railway bridge under the passage of railway traffic is predicted and compared with experimental measurements in a view to asses the adequacy of the numerical model.

2 Bridge description

The structure under study, taken as a representative example, is a double track bridge which belongs to the HS railway line Sevilla-Madrid in Spain. It is composed of three identical SS spans of 24.9m length measured between support centres. Each deck, with a extreme skew angle $\beta = 134°$, is made of a reinforced cast-in-situ concrete slab of 0.30m thick and 11.6m width, resting on five 2.05m high pre-stressed concrete I girders. The ends of these longitudinal girders at the supports are braced by a concrete cast-in-situ transverse diaphragm of rectangular cross section. The bridge substructure consist on two external abutments and two internal supports where the girders rest on laminated rubber bearings. In addition, identical elastic bearings restrict the transverse movement of the external girders. The bridge deck accommodates two ballasted tracks with UIC gauge. The UIC60 rails are supported on railpads and fixed to monoblock concrete sleepers separated 0.60m. Additionally, the deck contains sidewalks and handrails along the slab edges.

On may 2019 the authors performed an experimental campaign to characterise the bridge modal parameters and its dynamic response under operating conditions. Fifteen Endevco model 86 piezoelectric accelerometers with a nominal sensitivity of 10V/g were installed in the first span (the closest span to Madrid) underneath the girders (see Figure 1), and the vertical response was measured under ambient vibration and several train passages. It should be highlighted that only one span was instrumented for inaccessibility reasons at the site. For more details of the experimental campaign the reader is referred to [11].

In Figure 2 the first five experimental natural frequencies (f_i^{exp}), mode shapes and modal damping ratios (ζ_i^{exp}) are included. The frequencies and modal shapes were identified from ambient vibration applying the stochastic subspace identification technique [12]. Modal dampings were obtained from the free vibration

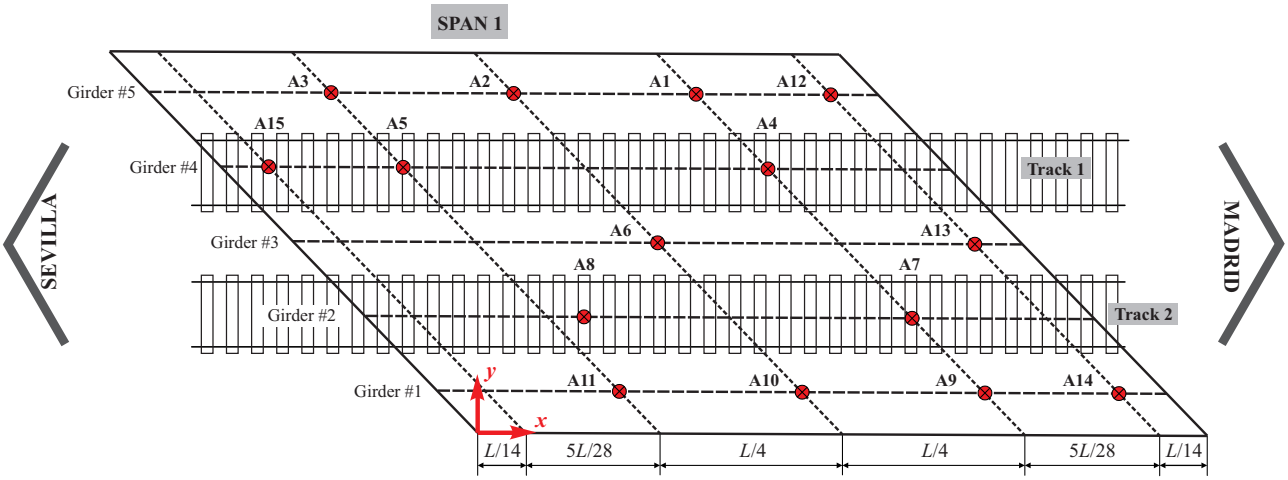

Figure 1: Sensors layout at span 1.

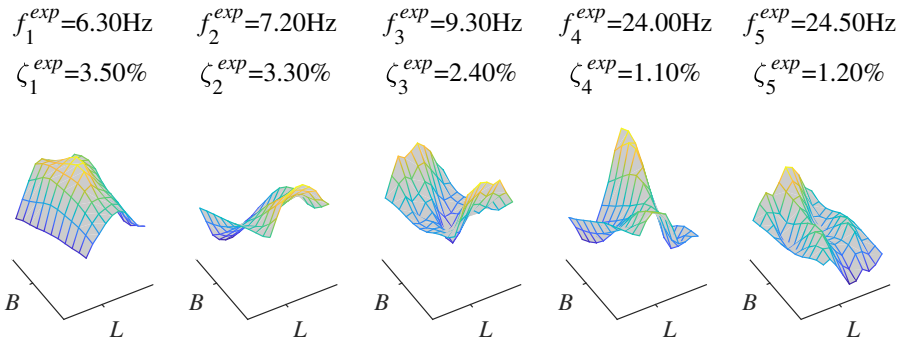

Figure 2: First five experimental modes, natural frequencies and free vibration damping ratios identified from experimental campaign.

response left by the train passage. As can be seen in Figure 2, the lowest mode in frequency order corresponds to the first longitudinal bending mode, while the second and third are associated to the first torsion and first transverse bending mode, respectively. Finally, the fourth and fifth modes, with similar frequencies, appear to be a second torsion and second transverse bending modes, respectively.

3 Numerical model

A 3D continuous finite element track-bridge interaction model of the full bridge is implemented in ANSYS. The model includes a track extension of 15m over the embankment before and after the bridge, which was considered adequate according to a convergence test performed on the modal parameters. The main features of the model are summarised in what follows:

- The slabs, diaphragms and longitudinal girders at each span are meshed with shell FE with 6 degrees of freedom (DOF) per node (SHELL181).
- For the laminated rubber bearings located underneath the girders, solid FE (SOLID185) of isotropic material are used, considering their real dimensions. In addition, the elastic bearings which restrict the transverse displacement of the external girder at each span are modelled using spring elements (COMBIN14).
- As per the track, Timoshenko beam elements with 6 DOF per node (BEAM188) are used for the

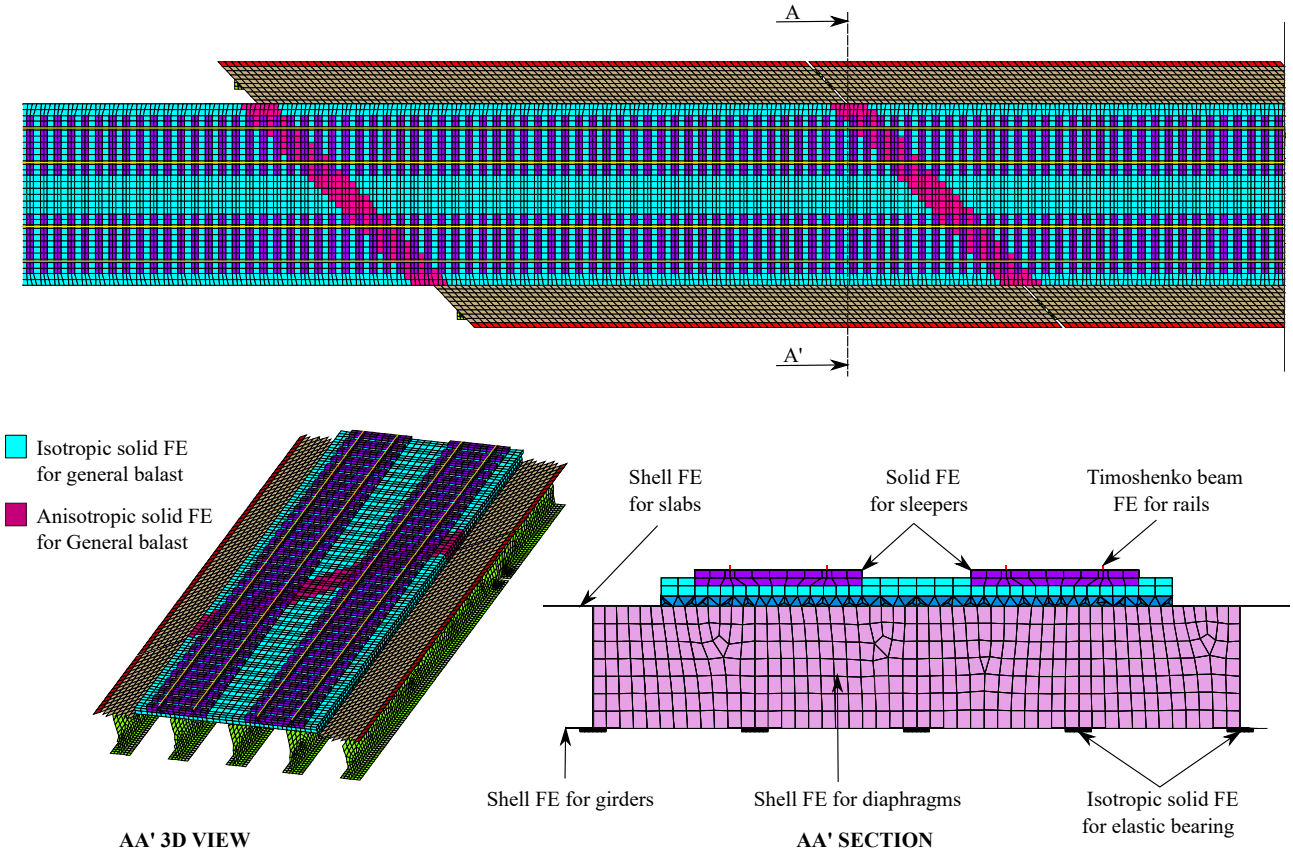

Figure 3: Detail of the bridge mesh.

rails, while the sleepers are discretised using solid FE (SOLID185) with 3 DOF per node. The rails are connected to the sleepers through discrete spring-damper FE (COMBIN14), representing the rail pads.

- The ballast layer is meshed with solid elements (SOLID185), which is divided into (i) a non degraded region of isotropic elastic behaviour; and (ii) a degraded region, placed in the vicinity of the transverse joint between the spans,with transversely isotropic material behaviour. With this approach different interlocking mechanisms of the ballast granules in the out-of-plane (vertical) and in the in-plane directions (horizontal) can be considered, associated to the possible degradation of this region.
- The non-structural elements are included in the model as a dead weight. Thus, the weight of the sidewalks is included in the model as an added distributed mass in the corresponding areas and the handrails are included in the model as lumped masses (MASS21).
- Under the track extension, a subgrade layer is included that is meshed with solid elements (SOLID185) of isotropic material.
- For the train excitation a constant moving load model is adopted, neglecting therefore the vehicle-bridge interaction (VBI).

Details of the bridge mesh are shown in Figure 3. The boundary conditions adopted in the FE model are: (i) the rotation of the rails in the longitudinal direction is restrained; (ii) the three translations of the nodes from the bottom surface of the subgrade layer are restrained; (iii) at both YZ planes that limit the track extensions vertically the three translations of the ballast and subgrade nodes are restrained as well; (iv) the vertical displacements at the bottom surface of the elastic bearings are restrained; (iv) along one abutment, the horizontal displacements (UX and UY) of the central node at the lower surface of the elastic bearings are also restrained.

With the previous considerations, the numerical model contains 854000 elements and 550033 nodes, which correspond to 2251700 DOF.

4 Model calibration

The numerical model of the bridge was calibrated in successive steps based on static and dynamic experimental results, that will be described in what follows. Tables 1 and 2 list all the model parameters used in the numerical idealisation of the bridge, in which the following nomenclature is used: E, G, ν, ρ and m stand for elastic and shear modulus, Poisson's ratio, mass density and linear distributed mass. Also, X, Y and Z refer to the longitudinal direction (parallel to the track), transverse and vertical directions, respectively. In the case of the rails, I_{yr} refers to the second moment of inertia of the cross-section with respect to Y. Concerning the track components,the spring-dashpot discrete properties of the rail pads K_p and C_p are provided. The sleepers dimensions (length l_{sl}, width w_{sl}, height h_{sl}) and total mass M_{sl} is considered according to [13]. In the ballast properties, h_b is the height of the ballast layer underneath the sleepers. The total ballast thickness is $h_b + h_{sl}/2$ which is assumed constant and uniform over the platform. A total thickness of 44cm is considered based on the technical drawings and in-situ inspection.

Notice that the main ballast presents isotropic elastic properties E_b and ν_b identical in the three directions, while the degraded ballast elastic constants are expressed as E_{bI}, G_{bIJ} and ν_{bIJ}, where I and J refer to the spatial directions X, Y and Z. The degraded ballast behaviour is defined as transversely isotropic with five independent elastic constants:

$$E_{bX} = E_{bY} \qquad E_{bZ} \qquad G_{bXZ} = G_{bYZ} \qquad \nu_{bXY} \qquad \nu_{bXZ} = \nu_{bYZ} \tag{1}$$

In Equation 1, $E_{bX} = E_{bY}$ are the in-plane elastic moduli, E_{bZ} and $G_{bXZ} = G_{bYZ}$ the out-of-plane elastic and shear moduli, respectively, and ν_{bXY} and $\nu_{bXZ} = \nu_{bYZ}$ the Poisson's ratios. Finally, R_{eb}=R_{ebt} are factors that multiply the vertical ans transverse elastic bearings modulus of elasticity in the case of dynamic loads.

First of all, the elastic modulus of the neoprene bearings (E_{eb}) was estimated in order to reproduce the experimental static deflection measured during the proof load test performed on the structure in 1991, before the bridge opening [14]. Secondly, the remaining model parameters which determination entails more uncertainty were subjected to a preliminary sensitivity analysis in a view to select the most influencing ones on the modal response of the structure, in terms of natural frequencies and mode shapes. The chosen parameters for this step are those for which a sensitivity analysis range is provided in Tables 1 and 2 (12 parameters). At the end of this step, 8 parameters exhibited a significant influence on the modal properties of the structure. Finally, the last step comprises an automated optimization procedure implemented in ANSYS-MATLAB based on the minimisation of an objective function under variations of the eight parameters selected in step 2, through a genetic algorithm (GA). Again, the chosen parameters are those for which a range of variation for the optimisation step is specified in Tables 1 and 2.

The objective function to be minimised through the GA (see Equation 2) involves the relative difference between the numerical and experimental frequencies of the paired modes (see Equation 3) and the Modal Assurance Criterion (MAC) [15] (see Equation 4). The five modes identified from ambient vibration were included in the updating step and the eight model parameters indicated in Equation 2 were subjected to variations ($E_s, E_g, E_b, E_{bX} = E_{bY}, \rho_s, \rho_g, \rho_b$ and $R_{eb} = R_{ebt}$).

$$F_{obj}(E_s, E_g, E_b, E_{bX} = E_{bY}, \rho_s, \rho_g, \rho_b, R_{eb} = R_{ebt}) = \sum_{i=1}^{5} \left| \frac{e_{100\%,i,j}}{100} \right| + \sum_{i=1}^{5} (1 - MAC_{i,j}) \tag{2}$$

$$e_{100\%,i,j} = \frac{f_i^{exp} - f_j^{num}}{f_i^{exp}} \cdot 100 \tag{3}$$

$$\text{MAC}_{i,j} = \frac{\left(\Phi_i^{exp,T} \cdot \Phi_j^{num}\right)^2}{\left(\Phi_i^{exp,T} \cdot \Phi_i^{exp}\right) \cdot \left(\Phi_j^{num,T} \cdot \Phi_j^{num}\right)} \tag{4}$$

In the previous equations, *exp* and *num* denote experimental and numerical, Φ_i^{exp} and Φ_j^{num} are the i-th and j-th experimental and numerical mode vectors, respectively, f_i^{exp} and f_j^{num} the corresponding natural frequencies and T indicates transpose.

Tables 1 and 2 also lists the final or updated values for each model parameter after performing the calibration process. The choice of the initial values and lower and upper bounds for both the sensitivity and optimisation steps is based on engineering considerations, the level of uncertainty on the particular track-bridge system properties and on reference values found in the literature.

Table 1: Track model parameters: initial values, ranges of variation and final values.

Bridge component	Notation	Initial value	Sensitivity analysis range	Optimisation range	Final value	Unit
Rail UIC60	E_r	$2.10 \cdot 10^{11}$	-	-	$2.10 \cdot 10^{11}$	Pa
	I_{yr}	$3038 \cdot 10^{-8}$	-	-	$3038 \cdot 10^{-8}$	m^4
	m_r	60.34	-	-	60.34	kg/m
Rail pads	K_p	$1.00 \cdot 10^8$	-	-	$1.00 \cdot 10^8$	N/m
	C_p	$7.50 \cdot 10^4$	-	-	$7.50 \cdot 10^4$	Ns/m
Sleepers	E_{sl}	$3.60 \cdot 10^{10}$	-	-	$3.60 \cdot 10^{10}$	Pa
	ν_{sl}	0.3	-	-	0.3	-
	w_{sl}	0.30	-	-	0.30	m
	l_{sl}	2.60	-	-	2.60	m
	h_{sl}	0.24	-	-	0.24	m
	M_{sl}	320	-	-	320	kg
Ballast	h_b	0.32	-	-	0.32	m
	$\boldsymbol{E_b}$	$1.10 \cdot 10^8$	$[-30, +30]\%$	$[-30, +30]\%$	$1.10 \cdot 10^8$	Pa
	ν_b	0.3	-	-	0.3	-
	$\boldsymbol{\rho_b}$	1800	$[-30, +30]\%$	$[-30, +30]\%$	1806	kg/m^3
Degraded ballast	$\boldsymbol{E_{bX} = E_{bY}}$	$1.10 \cdot 10^8$	$[-30, +30]\%$	$[-30, +30]\%$	$9.23 \cdot 10^7$	Pa
	E_{bZ}	$1.10 \cdot 10^8$	$[-30, +30]\%$	-	$1.10 \cdot 10^8$	Pa
	G_{bYZ}=G_{bXZ}	$4.23 \cdot 10^7$	$[-30, +30]\%$	-	$4.23 \cdot 10^7$	Pa
	ν_{bXY}=ν_{bYX}	0.2	-	-	0.2	-
	ν_{bXZ}=ν_{bYZ}	0.2	-	-	0.2	-
	$\boldsymbol{\rho_b}$	1800	$[-30, +30]\%$	$[-30, +30]\%$	1806	kg/m^3
Subgrade layer	E_f	$9.00 \cdot 10^7$	-	-	$9.00 \cdot 10^7$	Pa
	ν_f	0.3	-	-	0.3	-
	ρ_f	1800	-	-	1800	kg/m^3

Table 3 shows the results of the model calibration in terms of numerical frequencies (f_j^{num}), frequency differences ($e_{100\%,i,j}$) and MAC numbers of the paired numerical modes. As can be seen, the first longitudinal bending, torsion and transverse bending modes are reproduced with frequency differences below 5.6% and average MAC number 0.92. The torsion mode, whose contribution is expected to be significant given the obliquity of the deck and eccentricity of the tracks is specially well calibrated. The fourth and fifth modes present very close frequencies, near 24Hz and less accurate adjustment is achieved in these cases.

Table 2: Deck model parameters: initial values, ranges of variation and final values.

Bridge component	Notation	Initial value	Sensitivity analysis range	Optimisation range	Final value	Unit
Girders	$\boldsymbol{E_g}$	$3.74 \cdot 10^{10}$	$[-20, +20]\%$	$[-20, +20]\%$	$4.32 \cdot 10^{10}$	Pa
	ν_g	0.2	-	-	0.2	-
	$\boldsymbol{\rho_g}$	$2.23 \cdot 10^3$	$[-08, +08]\%$	$[-08, +08]\%$	$2.23 \cdot 10^3$	kg/m^3
Slabs	$\boldsymbol{E_s}$	$3.19 \cdot 10^{10}$	$[-20, +30]\%$	$[-20, +30]\%$	$2.55 \cdot 10^{10}$	Pa
	ν_s	0.2	-	-	0.2	-
	$\boldsymbol{\rho_s}$	$2.50 \cdot 10^3$	$[-08, +08]\%$	$[-08, +08]\%$	$2.50 \cdot 10^3$	kg/m^3
Diaphragms	E_{dph}	$2.55 \cdot 10^{10}$	$[-20, +30]\%$	-	$2.55 \cdot 10^{10}$	Pa
	ν_{dph}	0.2	-	-	0.2	-
	ρ_{dph}	$2.50 \cdot 10^3$	-	-	$2.50 \cdot 10^3$	kg/m^3
Handrails	m_b	50	-	-	50	kg/m
Sidewalks	ρ_f	195	-	-	195	kg/m
Vertical elastic bearing	E_{eb}	$2.57 \cdot 10^7$	-	-	$2.57 \cdot 10^7$	Pa
	ν_{eb}	0.49	-	-	0.49	-
	ρ_{eb}	1230	-	-	1230	kg/m^3
	$\boldsymbol{R_{eb}}$	1.25	$[+00, +60]\%$	$[+00, +60]\%$	1.83236	-
	w_{eb}	0.40	-	-	0.40	m
	l_{eb}	0.33	-	-	0.33	m
	h_{eb}	0.049	-	-	0.049	m
Transverse elastic bearing	K_{eb}	$2.95 \cdot 10^7$	-	-	$2.95 \cdot 10^7$	N/m
	R_{ebt}	1.25	$[+00, +60]\%$	-	1.83236	-

Table 3: Experimental and numerical frequencies for modes under 30 Hz. Frequency differences and MAC numbers of the paired modes after calibration.

Mode (i)	1	2	3	4	5
f_i^{exp} (Hz)	6.30	7.20	9.30	24.00	24.50
f_j^{num} (Hz)	6.19	6.80	9.79	18.39	24.92
$e_{100\%,i,j}$ (-)	1.70	5.51	-5.31	23.35	-1.72
$MAC_{i,j}$ (-)	0.93	0.96	0.88	0.79	0.57

5 Sensitivity analysis

A comprehensive sensitivity analysis is presented on two geometrical features of the bridge that may affect the dynamic response: (i) the skew angle; and (ii) the transverse diaphragms configuration. With regard to the diaphragms, three configurations are considered based on real scenarios that can be found in the existing structures which are: (a) cast-in-situ concrete diaphragms fully connected to the girders web, top flange and upper slab (FD); (b) poorly built diaphragms connected to the girders web but not to the upper slab (PD); (c) absence of diaphragms (ND). The aim of this sensitivity analysis is to evaluate the influence of these properties and their combinations on the maximum vertical response under train passages. In order to isolate the effect of these geometrical aspects among others, the study is performed considering only one bridge span in the numerical model and including the track extension on both sides. The updated bridge properties shown in Tables 1 and 2 are considered as reference case for this analysis. Twenty five post-process points are defined (see Figure 4) located underneath the girders and uniformly distributed to evaluate the dynamic response of the bridge under variations of the geometrical parameters.

The dynamic response of the one-span bridge under different levels of skewness and transverse diaphragm configurations is analysed under the circulation of the 10 trains of the High Speed Load Model-A (HLSM-A) defined in EC1. The trains cross the bridge along track 2 at constant speeds in the range $[144 - 421.2]$km/h

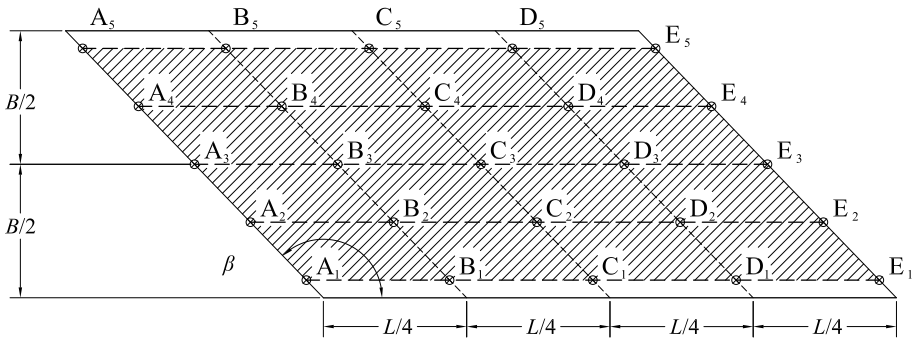

Figure 4: Post-process points.

in 3.6km/h increments. Herein 9 bridge model variants are evaluated, taking into account three levels of obliquity ($\beta = [90, 112, 134]^\circ$) and the three diaphragms configurations previously defined (FD, PD and ND). The dynamic problem is solved by Modal Superposition of the first three modes of vibration (first longitudinal bending, first torsion and first transverse bending modes) in the time domain. The equations of motion are numerically integrated by the Newmark-Beta Linear Acceleration algorithm. The time step is defined as $1/50$ times the smallest period of interest. A modal damping ratio of 1% is admitted according to EC1 for the particular material and span length. Finally, envelopes of maximum acceleration $|a_{max}|$ at the 25 points of post-process are computed.

Table 4: Maximum vertical acceleration, post-process point, train and travelling speed for $\beta = [90, 112, 134]^\circ$ and diaphragm configurations FD, PD and ND.

Diaphragm conf.	$\lvert a_{max}\rvert$ (m/s^2)	$\beta = 90^\circ$	$\beta = 112^\circ$	$\beta = 134^\circ$
FD	value	4.322	4.189	3.234
	Fig. 4 point	C2	C2	C1
	train/V(km/h)	A3/421.2	A3/421.2	A10/396.0
PD	value	4.312	4.186	3.343
	Fig. 4 point	C2	C2	C1
	train/V(km/h)	A3/421.2	A3/421.2	A10/396.0
ND	value	4.333	4.130	3.580
	Fig. 4 point	C2	C2	C1
	train/V(km/h)	A3/421.2	A3/421.2	A10/392.4

In Table 4 the maximum acceleration reached in each of the 9 cases of study is included, along with the location where it takes place, the train and the speed. The overall maximum acceleration reaches 4.33m/s^2, higher than the limit prescribed in EC [1] for ballasted track bridges. Nevertheless, the design speed considered corresponds to a maximum speed in the railway line section of 350km/h (see vertical red dashed line on Figure 6) which exceeds the actual one (300km/h). For the decks with $\beta = 90^\circ$ and $\beta = 112^\circ$, train HSLM-A3 leads to the maximum acceleration at the maximum speed considered and at point C2, under the loaded track. This is due to the excitation of a first resonance of the fundamental mode. In the bridges with $\beta = 134^\circ$ this resonant speed falls out of the analysis speed window and the maximum acceleration happens at C1 (border girder) under the circulation of HSLM-A10 train, which excites a second resonance of the torsion mode at 396km/h. The theoretical resonant speeds for these two trains in the FD case are given by:

$$V_{i=1,j=1}^{rA3,90^\circ} = \frac{d_k \cdot f_1}{j} = \frac{20\text{m} \cdot 5.83\text{Hz}}{1} = 116.6\text{m/s} = 419.8\text{km/h} \tag{5}$$

$$V_{i=2,j=2}^{rA10,134^\circ} = \frac{d_k \cdot f_2}{j} = \frac{27\text{m} \cdot 8.15\text{Hz}}{2} = 110.03\text{m/s} = 395.9\text{km/h} \tag{6}$$

In Figure 5 envelopes of maximum acceleration for the 10 HSLM-A trains and for the complete range of

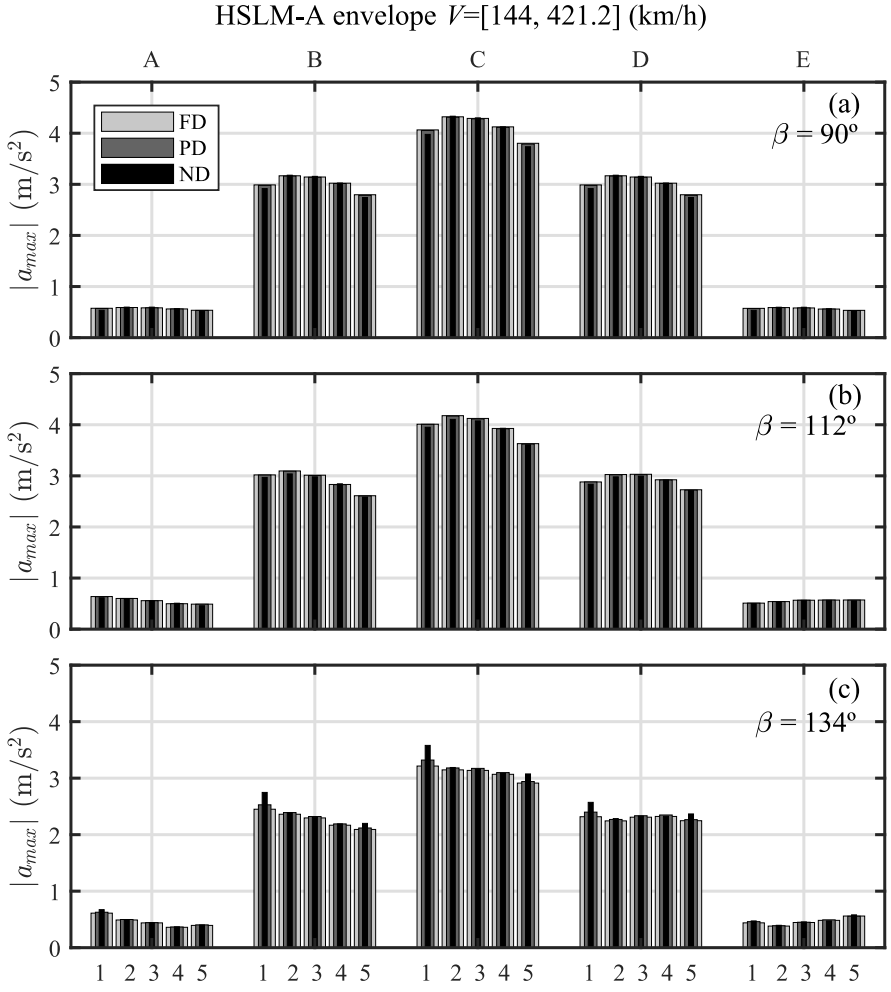

Figure 5: Maximum estimated acceleration on post-process points under passage of the HLSM-A trains with a speed range of $[154 - 421.2]$ km/h. Thicker bars FD, medium width bars PD and thinner bars ND.

velocities are represented at the 25 postprocess points. A-E defines the cross section and 1-5 the particular point (see Figure 4). Subplots (a), (b) and (c) correspond to skew angles of $90°$, $112°$ and $134°$, while light grey, dark grey and black stand for the three diaphragm configurations FD, PD and ND, respectively. From the analysis of the figure it can be concluded that (i) generally speaking, the overall maximum acceleration reduces with the deck obliqueness; (ii) the overall maximum response always takes place at mid-span, consistently with the modes accounted for in the analysis; (iii) in straight bridges or bridges with small obliqueness, the diaphragm configuration is negligible. However, for relevant levels of skewness, decks without transverse diaphragms exhibit higher vertical accelerations at the border girders, especially if the participation of the torsion mode is significant, as it is in this case.

Finally, in Figure 6 envelopes of maximum acceleration for the 10 HSLM-A trains at point C1 are plotted in terms of the circulating velocity, considering separate modal contributions. Black, dark grey and light grey traces correspond to the response computed accounting for the participation of the fundamental, first and second and the first three modes, respectively. Associated to some of the resonant peaks, which are quite similar in all the plots, the train causing resonance, the mode under resonance i and the resonance order j are specified in Figure 6(b) with the nomenclature ATr(i, j), for Tr being the train number. It may be concluded that (i) the contribution of modes different from the longitudinal bending one is very relevant for speeds higher than 300km/h in all the cases. This is related to second resonances ($j = 2$) of the torsion mode ($i = 2$) excited by the trains with the longest characteristic distances (A7 to A10). These results show

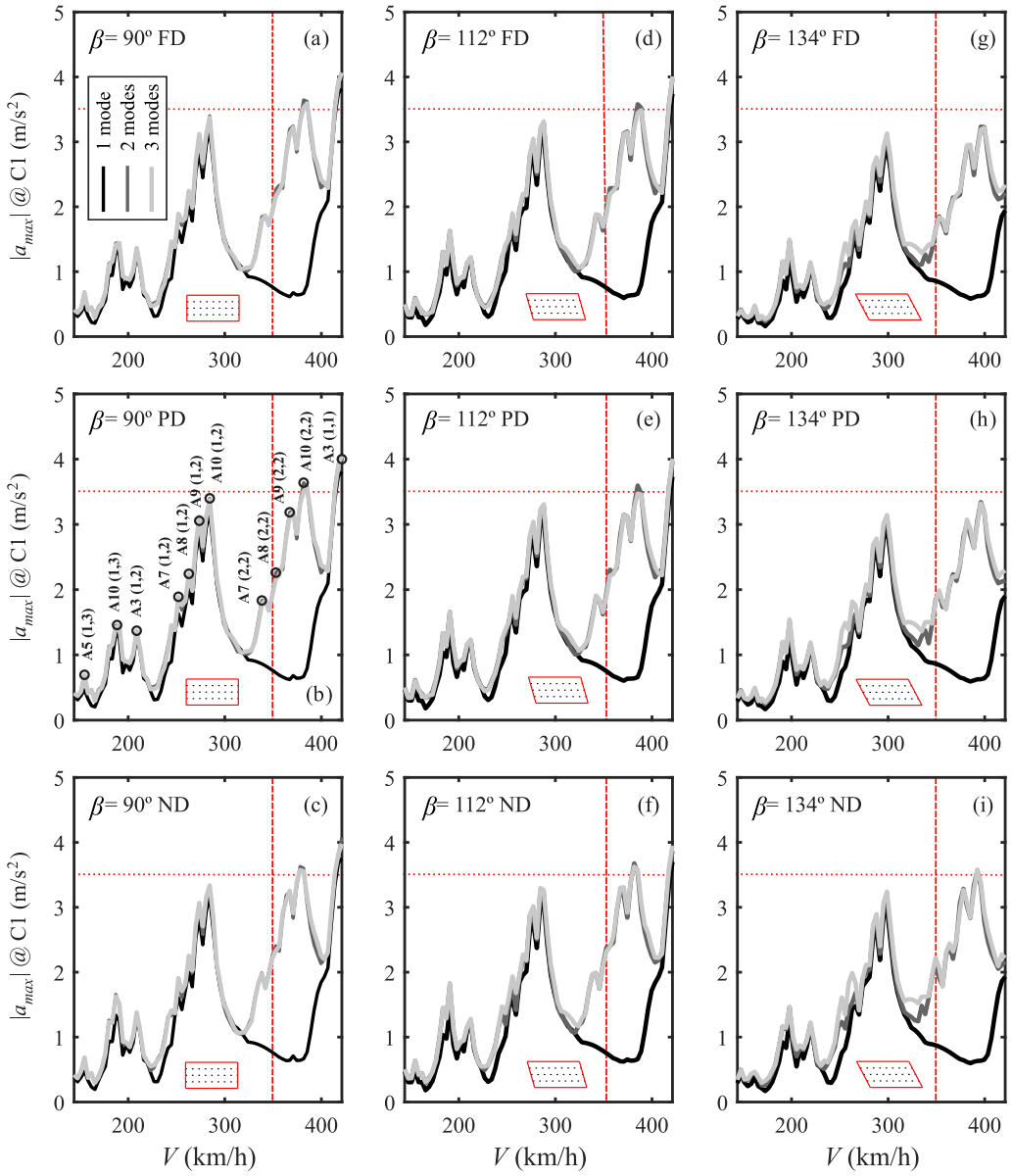

Figure 6: Maximum estimated acceleration on point C1 under passage of the HLSM-A trains with a speed range of $[144 - 421.2]$ km/h.

the importance of the use of three-dimensional structural models that not only account for the longitudinal bending of the bridge; (ii) the contribution of the transverse bending modes is visible only for the highest obliquity level; (iii) the overall maximum acceleration reduces with the skew angle mainly because the first resonance of the fundamental mode falls out of the speed window in the case $\beta = 134°$ due to the increase in the fundamental frequency; (iv) the influence of the diaphragm configurations (FD vs PD) is negligible on the maximum acceleration, no matter the bridge obliqueness. Nevertheless, the total absence of these elements is relevant in oblique cases, leading to an increment of the maximum acceleration of approximately 10% in the cases evaluated.

6 Bridge response under train passages

During the experimental campaign performed on Jabalón bridge the vertical response in one of the bridge spans was registered under several train circulations. This section shows an experimental-numerical com-

parison of the vertical acceleration response at the sensors indicated in Figure 1, which were installed below the girders lower flange, under the passage of the train RENFE S104. This is a conventional train with distributed traction, composed by two locomotives and two passenger coaches with a characteristic distance of $d = 25.9$m. More details about the train configuration can be found in [11].

For the numerical predictions, the updated model of Jabalón Bridge including the three spans weakly coupled through the track is used. The bridge vertical response under the train passage is obtained by Modal Superposition, considering the contribution of modes under 30Hz. The equations of motion are numerically integrated in the time domain applying the Newmark-Linear Acceleration algorithm. The time step is defined as $1/50$ times the smallest period included in the analysis. Modal damping values identified from the free vibrations left by the trains (see Figure 2) are assigned to the paired modes and 1% is assigned to the remaining ones according to EC [5]. The experimental response is filtered applying two third-order Chebyschev filters with high-pass and low-pass frequencies of 1Hz and 30Hz respectively.

In Figure 7 the vertical acceleration response under RENFE S104 passage at 249km/h from Madrid to Sevilla along track 1 is represented (see Figure 1). Accelerometers A1, A3, A5 and A15 are selected, being A15 the closest to the Sevilla abutment. The acceleration response is plotted in the time domain (first column), frequency domain (second columns) and in one-third octave frequency bands (third column). Experimental results and numerical predictions are represented with black and grey traces, respectively.

This train axle scheme and travelling velocity does not induce resonance of any of the first three modes. The second and third resonance velocities of the first, second and third modes are theoretically $v_{i=1,j=2}^{rS104} = f_i \cdot d/j = f_1 \cdot d/2 = 294$km/h, $v_{2,3}^{rS104} = f_2 \cdot d/3 = 224$km/h and $v_{3,3}^{rS104} = f_3 \cdot d/3 = 289$km/h, which are distant from the actual speed of 249km/h. As resonance is not induced, several modal contributions participate in the vertical acceleration response of the bridge.

In the frequency domain plots (see Figure 7(e)-(h)) the numerical response matches perfectly the bogie passing frequency ($V/d = 2.67$Hz). The fitting of the bridge modes up to 22Hz is excellent both in frequency and in amplitude. The response is well represented even close to the abutment (accelerometer A15) which is not easy due to the dependence of the model on the boundary conditions, given the high obliquity of the deck. As was shown in the sensitivity analysis, the contributions of the first transverse and first torsion modes are quite relevant and highlight the necessity to use three-dimensional models to properly predict the dynamic response of these oblique double-track girder bridges. The time history response (see Figure 7(a)-(d)) is correctly predicted under free vibration. Under forced vibration the response is slightly underestimated by the numerical model due to the frequency contributions between $[25 - 30]$Hz where the model is not able to reproduce accurately, most probably related to the track irregularities. Despite of the founded differences on high frequency between experimental and numerical comparison, the vehicle-bridge-interaction and track irregularities were neglected because (i) admitting distributed loads model is a probable situation in engineering consultancies; (ii) only the bridge response is of interest; (iii) VBI effects are mainly relevant at resonance; (iv) there is not available technical information about suspension values for S104 train.

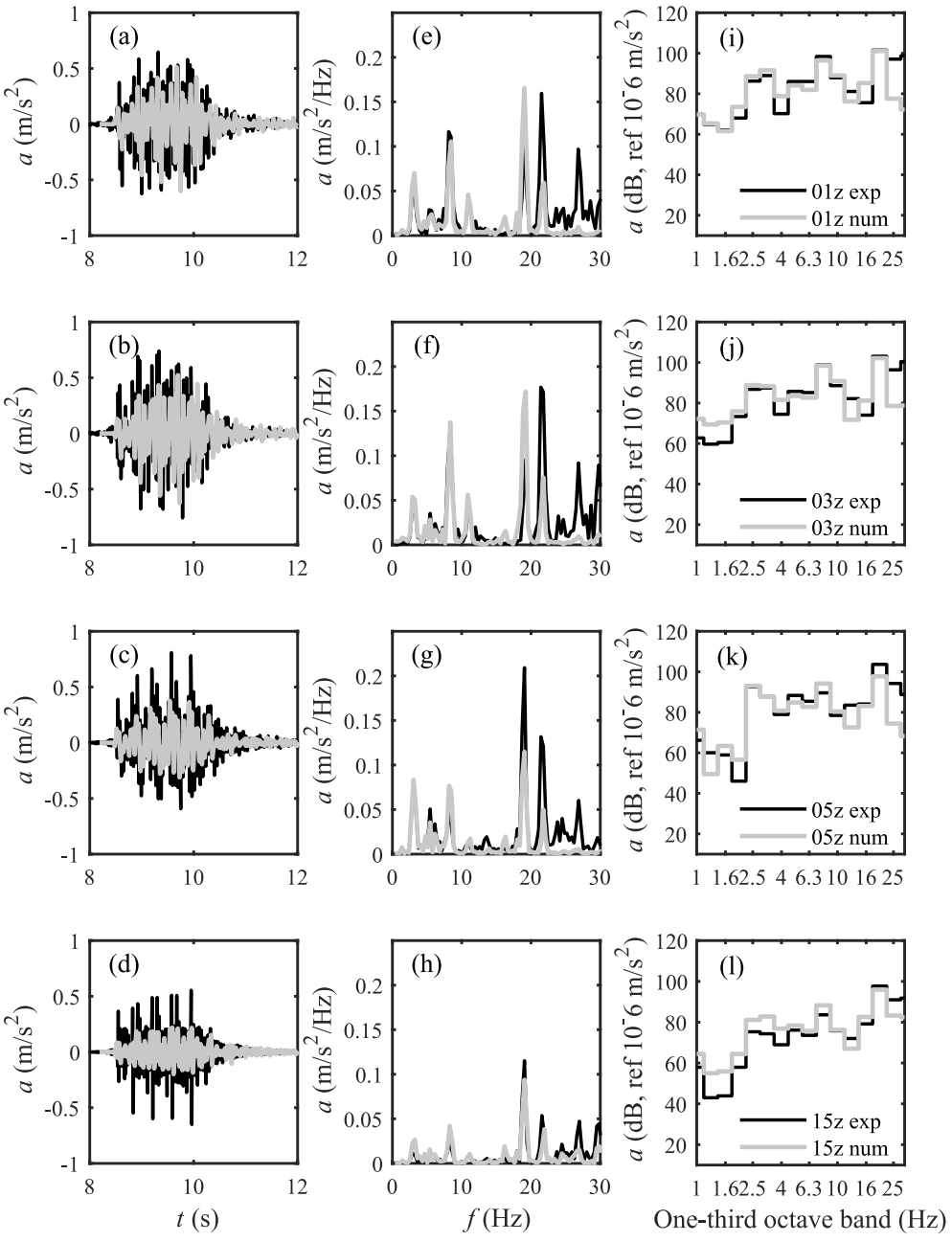

Figure 7: Time history, frequency content and one-third octave band comparison of the accelerations at points A1 A3 A5 and A15, induced by conventional train RENFE S104 on track 1 M-S at speed 249km/h.

7 Conclusions

In this work the dynamic response of skewed multi-span railway bridges composed by isostatic pre-stressed concrete girder decks is evaluated. In particular, the influence of two geometrical aspects usually neglected in the numerical models used in practical applications for the assessment of the Serviceability Limit State of vertical accelerations are investigated, which are: (i) the deck obliquity; (ii) the transverse diaphragms configuration. To this end, a 3D continuous finite element track-bridge interaction model of an existing skewed bridge belonging to the Spanish HS railway network is implemented. From this reference case, a set of model variants are envisaged to account for different skew angles and diaphragms configurations, to evaluate their influence on the bridge dynamic response under operating conditions.

From the sensitivity analysis performed, the following can be concluded:

- The overall maximum acceleration reduces with the deck obliqueness. This is mainly caused by the fact that the resonances of the fundamental mode that take place at the highest velocities considered fall out of the speed window when the skewness increases. This not being the case, the detected differences are lower.
- The contribution of modes different from the longitudinal bending one is very relevant for speeds higher than 300km/h. Therefore, the use of three-dimensional structural models that not only account for the longitudinal bending of the bridge is important for the evaluated bridge typologies.
- The influence of the diaphragm configuration (FD vs PD) on the vertical acceleration levels under train passages is negligible, for any level of obliqueness. However, the total absence of these elements is relevant in oblique cases, leading to an increment in the maximum acceleration of approximately 10% in the cases evaluated.

Concerning the experimental-numerical comparison of the dynamic response of Jabalón HS railway bridge, the results have shown that the updated 3D finite element model reproduces with reasonable accuracy the dynamic response under the passage of a conventional train for frequency contents below 22Hz. In this regard, it is important to highlight that the numerical model neglects the vehicle-bridge interaction and therefore, also the track irregularities. The evaluated train passage is particularly interesting since the speed of circulation does not induce resonance. Therefore, a number of structural mode contributions different from the longitudinal bending ones participate in the vertical acceleration response. Particularly, the contribution of the first transverse and first torsion modes is quite relevant and highlights the importance of using 3D numerical models to properly predict the dynamic response of oblique double-track girder bridges.

Acknowledgements

The authors would like to acknowledge the financial support provided by the Junta de Andalucía and the European Social Fund through the contract USE-22311-R with Universidad de Sevilla, and also the Spanish Ministry of Science and Innovation under research project PID2019-109622RB-C2 and Generalitat Valenciana under research project AICO/2021/200.

References

[1] CEN, *EN 1991:2002+A1:2005 (E) Eurocode - Basis of structural design. Annex 2 - Application for bridges*. European Committee for Standardization, Brussels, 2005.

[2] UIC - International Union of Railways, "Rail bridges for speeds $>$ than 200km/h. ," *Final report. Part A. Synthesis of the results of D214 research*, vol. ERRI-D-214/RP9, 1999.

[3] W. Hoorpah, "Dynamic calculations of high-speed railway bridges in France – some case studies," in *Dynamics of High-Speed Railway Bridges*, T. &. Francis, Ed., no. 978-0-203-89540-5, Jun. 2008, pp. 133–146.

[4] L. Frýba, *Dynamics of railway bridges*. Thomas-Telford, 1996.

[5] CEN, *EN 1991-2:2003 Eurocode 1: Actions on Structures - Part 2: Traffic loads on bridges*. European Committee for Standardization, Brussels, 2003.

[6] P. Ryjácek, M. Polák, T. Plachý, J. Kaspárek, "The dynamic behaviour of the extremly skewed railway bridge 'oskar'," *Procedia Structural Integrity*, vol. 5, pp. 1051–1056, 2017.

[7] K. Nguyen, J. M. Goicolea, and F. Gabaldón, "Comparison of dynamic effects of high-speed traffic load on ballasted track using a simplified two-dimensional and full three-dimensional model," *Proceedings of the Institution of Mechanical Engineers, Part F: Journal of Rail and Rapid Transit*, vol. 228, no. 2, pp. 128–142, 2014. [Online]. Available: https://doi.org/10.1177/0954409712465710

[8] E. Moliner, A. Romero, P. Galvín, and M. Martínez-Rodrigo, "Effect of the end cross beams on the railway induced vibrations of short girder bridges," *Engineering Structures*, vol. 201, p. 109728, 2019.

[9] E. Axelsson, A.Syk, M. Ülker-Kaustell, J-M Battini, "Effect of axle load spreading and support stiffness on the dynamic response of short span railway bridges," *Structural Engineering International*, no. 24, pp. 457–465, 2014.

[10] L. Bornet, A. Andersson, J. Zwolski, J-M Battini, "Influence of the ballasted track on the dynamic properties of a truss railway bridge," *Structure and Infrastructure Engineering*, no. 11, pp. 796–803, 2015.

[11] P. Galvín, A. Romero, E. Moliner, G. De Roeck, and M. Martínez-Rodrigo, "On the dynamic characterisation of railway bridges through experimental testing," *Engineering Structures*, vol. 226, p. 111261, 2021.

[12] E. Reynders, "System identification methods for (operational) modal analysis: review and comparison," *Archives of Computational Methods in Engineering*, vol. 19, no. 1, pp. 51–124, 2010.

[13] G. d. E. Ministerio de fomento, "Instrucción de acciones a considerar en puentes de ferrocarril." 2010.

[14] INTEMAC, "Informe de resultados y conclusiones de las actividades de inspección técnica y prueba de carga realizadas en la estructura del puente P.K. 11+184, del tramo El Emperador-Ciudad Real sobre el río Jabalón," 1991.

[15] R. J. Allemang, "The modal assurance criterion - twenty years of use and abuse," *Journal of Sound and Vibration*, no. 37, pp. 14–21, 2003.